Wavelength, Concentration, and Distance Dependence of Nonradiative Energy Transfer to a Plane of Gold Nanoparticles

Xia Zhang,[†] Cristian A. Marocico,[†] Manuela Lunz,[†] Valerie A. Gerard,[‡] Yurii K. Gun'ko,[‡] Vladimir Lesnyak,[§] Nikolai Gaponik,[§] Andrei S. Susha,[⊥] Andrey L. Rogach,[⊥] and A. Louise Bradley[†,*]

[†]School of Physics and CRANN and [‡]School of Chemistry and CRANN, Trinity College, Dublin 2, Ireland, [§]Physical Chemistry, TU Dresden, Bergstrasse 66b, 01062 Dresden, Germany, and [⊥]Department of Physics and Materials Science and Centre for Functional Photonics (CFP), City University of Hong Kong, Hong Kong S.A.R.

ABSTRACT

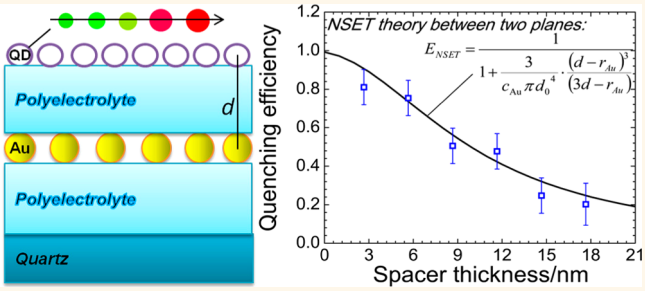

Nonradiative energy transfer to metal nanoparticles is a technique used for optical-based distance measurements which is often implemented in sensing. Both Förster resonant energy transfer (FRET) and nanometal surface energy transfer (NSET) mechanisms have been proposed for emission quenching in proximity to metal nanoparticles. Here quenching of emission of colloidal quantum dots in proximity to a monolayer of gold nanoparticles is investigated. Five differently sized CdTe quantum dots are used to probe the wavelength dependence of the quenching mechanism as their emission peak moves from on resonance to off resonance with respect to the localized surface plasmon peak of the gold nanoparticle layer. The gold nanoparticle concentration and distance dependences of energy transfer are discussed. Photoluminescence quenching and lifetime data are analyzed using both FRET and NSET models and the extracted characteristic distances are compared with theory. Good agreement with FRET theory has been found for quantum dots with emission close to the localized surface plasmon resonance, though larger than expected Förster radii are observed for quantum dots with emission red-shifted with respect to the localized surface plasmon peak. Closer agreement between experimental and theoretical characteristic distances can be found across the full wavelength range within a NSET approach.

KEYWORDS: surface plasmons · fluorescence quenching · gold nanoparticles · quantum dots · Förster resonance energy transfer · nanometal surface energy transfer

Nanosensors based on the localized surface plasmon (LSP) induced quenching of fluorophores continue to attract a lot of interest.[1−3] In particular the distance dependence of the quenching process of molecular dyes[4] and colloidal quantum dots (QDs)[1,5] created the basis for a plasmon-ruler with an extended range compared to the previously proposed nanoruler[6] based on FRET between two fluorescent molecules.[7,8] A good understanding of the distance dependence is important for the design of nanosensors as the transfer efficiency, and consequently the sensitivity of the nanosensor, drops off strongly with increasing distance. Distance-dependent quenching in single fluorophore−metal nanoparticle (MNPs) pairs has been studied using variable length polypeptide[5] and DNA strands[4,9] and more recently gold nanoparticles (Au NPs) incorporated in DNA origami.[10] The impact of the spectral overlap, of the LSP resonance and the emission spectrum of the fluorophore, on the quenching efficiency by the MNP has been analyzed by varying the molecular dye or QD emission or the Au NP size.[1,11,12] It is important to investigate the concentration dependence of the LSP quenching process, as this can also impact on the sensitivity of nanosensors. By understanding the distance and concentration dependences of a particular MNP−fluorophore system, the optimum conditions for high sensitivity can be determined. The distance, wavelength, and concentration dependences of the quenching process of molecular dyes and QDs by MNPs can be analyzed using theories describing nonradiative energy transfer between dipoles within both FRET[13−15] and NSET formalisms.[4,5,10]

For many applications semiconductor QDs offer advantages over the typically used molecular dyes, such as their narrow and tunable emission lines, higher photostability and high quantum yields.[16,17] In addition to the distance dependence of the QD emission quenching by near-by metal NPs,[1,5] the formation of oppositely charged QD−metal

* Address correspondence to bradlel@tcd.ie.

Received for review August 17, 2012 and accepted September 13, 2012.

Published online September 13, 2012
10.1021/nn303756a

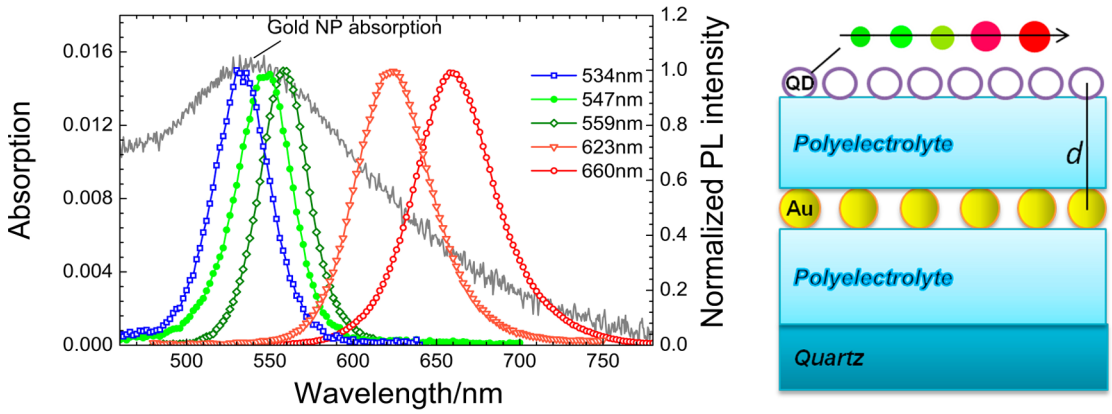

Figure 1. Photoluminescence (PL) spectra of monolayers of each of the five different sizes thioglycolic acid (TGA) stabilized CdTe QDs (right axis), and the absorption spectrum (left axis) of a gold nanoparticle (NP) layer, with a concentration of c_{Au} = 0.11 × 10^{17} m^{-2}, (gray line). A schematic of the bilayer structure is also shown.

NP nanoassemblies in solution has been investigated, and the observed QD emission quenching as a function of the QD−metal NP ratio was explained by energy transfer in predominantly single QD−single metal NP structures.[18] The dependence of the QD emission quenching efficiency on the spectral overlap with respect to the LSP resonance and the MNP concentration are important characteristics for optimization of QD−metal based nanosensors and other photonic devices.[19,20] In particular, quenching of QD emission by a plane of MNPs has not been comprehensively studied. For example, the authors reported on LSP enhancement of energy transfer between planes of QDs, and in such a system quenching of the QD emission by a plane of MNPs is a competing mechanism.[21,22] Energy transfer from dyes to a nanostructured silver film, formed by the accumulation of particles of various sizes ranging from nanometers to micrometers, has also been recently reported.[14] Apart from its relevance to sensing and photonic device applications, by using a planar geometry the Au NP−QD separation as well as the Au NP concentration can be independently controlled. The wavelength dependence can be probed by using differently sized QDs. To the best of our knowledge this is the first characterization of the QD−metal energy transfer mechanism as a function of the separation, MNP concentration, and emission wavelength in a planar geometry.

Here, the emission quenching in a CdTe QD−colloidal Au NP bilayer structure is examined. Distance and Au NP concentration dependences of the emission quenching are characterized for five different sizes of CdTe QDs, with peak emission wavelength varying from 534 to 660 nm (see Figure 1). The QD emission is tuned from on resonance to off resonance with respect to the LSP peak of the Au NP layer. The quenching is characterized using both photoluminescence (PL) spectra and PL decays. The distance and Au NP concentration dependences are compared with both FRET and NSET models. The different formalisms to describe nonradiative energy transfer for single emitter−MNP pairs have been reviewed elsewhere, here we will present details relevant to energy transfer to a plane of MNPs.[5,11] A schematic of the structure is shown as an inset in Figure 1.

The nonradiative energy transfer efficiency is given by

$$E_{NRET} = \frac{k_{ET}}{k_r + k_{nr} + k_{ET}} \quad (1)$$

where k_r, k_{nr}, and k_{ET} are the radiative recombination rate, the nonradiative recombination rate, and the nonradiative energy transfer rate, respectively. Within the FRET formalism, the QD and Au NP are approximated as point dipoles, and for a single QD−Au NP pair the energy transfer rate can be expressed as

$$k_{FRET} = \tau_D^{-1}\left(\frac{R_0}{r_{DA}}\right)^6 \quad (2)$$

where $\tau_D = (k_{nr} + k_r)^{-1}$ is the intrinsic lifetime of the quantum dot emission decay, that can be determined from time-resolved photoluminescence measurements, r_{DA} is the center to center separation between the QD and Au NP. R_0, the Förster radius, is the characteristic distance at which the energy transfer efficiency is 50%. The Förster radius is given by[23,24]

$$R_0 = 0.0211\left(\frac{\kappa^2 QY}{n^4} J\right)^{1/6} \quad (3)$$

where κ^2 is the orientation factor of the dipoles and has a value of $^2/_3$ for randomly oriented dipoles as in the structures considered in this paper. QY is the PL quantum yield of the QDs, n is the refractive index of the surrounding medium and $J = \int_0^\infty \hat{I}_{QD}(\lambda)\cdot\varepsilon_{AuNP}(\lambda)\lambda^4\, d\lambda$ is the spectral overlap of the area-normalized donor QD emission spectrum, $\hat{I}_{QD}(\lambda)$, and the acceptor Au NP extinction spectrum, $\varepsilon_{AuNP}(\lambda)$. The QD QY can be experimentally obtained by comparing the spectral properties of the QDs with those of a well-known luminescent reference such as Rhodamine 6G, as used here. In the case of bilayer structures, the rate of energy transfer to

the Au NP plane is expressed as

$$k_{FRET} = \tau_D^{-1} \sum_i \left(\frac{R_0}{r_i}\right)^6 \quad (4)$$

where r_i is the separation from the center of the QD to the center of each Au NP. Performing an integration over an infinite plane the energy transfer efficiency can be expressed as

$$E_{FRET} = \frac{1}{1 + \frac{2d^4}{c_{Au}\pi R_0^6}} \quad (5)$$

where c_{Au} is the Au NP concentration and $d = t + r_{QD} + r_{Au}$ is the separation between the QD monolayer and Au NP monolayer, which includes the spacer layer thickness, t, as well as the radii of the QD, r_{QD} and Au NP, r_{Au}. It can be seen that the FRET efficiency for a QD interacting with a plane of Au NP acceptors shows a d^{-4} dependence as opposed to the d^{-6} dependence observed for a single donor–acceptor pair.[25]

Within the NSET formalism, energy transfer for a single QD–Au NP pair is considered to occur from a donor point dipole QD to an infinite Au surface.[26] The energy transfer rate can be expressed as

$$k_{NSET} = \tau_D^{-1} \left(\frac{d_0}{r_{DA} - r_{Au}}\right)^4 \quad (6)$$

in which the separation between the QD and the Au surface includes only the QD radius and the spacer layer thickness, t. The characteristic distance for which the NSET efficiency is 50%, denoted as d_0, can be calculated from

$$d_0 = \left(0.225 \frac{QY}{\omega_{QD}^2} \frac{1}{\omega_F k_F} \frac{c^3}{n}\right)^{1/4} \quad (7)$$

where $\omega_F = 8.4 \times 10^{15}$ rad/s and $k_F = 1.2 \times 10^8$ cm^{-1} are the bulk gold angular frequency and Fermi vector, respectively, c is the speed of light, n is the refractive index of the medium, and ω_{QD} is the QD emission frequency.[4] The inclusion of the refractive index in this manner is justified by observing that the radiative decay rate in a medium of refractive index n is given by $k_r = nk_r^0$, where k_r^0 is the radiative decay rate in vacuum.

In the case of bilayer structures, with each QD–Au NP pair interaction treated within the NSET formalism, the rate of energy transfer to the Au NP plane is expressed as

$$k_{NSET} = \tau_D^{-1} \sum_i \left(\frac{d_0}{r_i - r_{Au}}\right)^4 \quad (8)$$

By integration the NSET efficiency can be expressed as

$$E_{NSET} = \frac{1}{1 + \frac{3}{c_{Au}\pi d_0^4} \cdot \frac{(d - r_{Au})^3}{(3d - r_{Au})}} \quad (9)$$

The nonradiative energy transfer efficiency for a QD interacting with a plane of Au NP acceptors within the NSET formalism shows a d^{-2} separation dependence as opposed to the d^{-4} dependence for FRET to a plane of acceptors.

RESULTS AND DISCUSSION

Bilayer structures with QDs and Au NPs were prepared by a layer-by-layer deposition technique. The colloidal Au NPs have an average diameter of 5.5 nm, and monolayers of different Au NP concentrations are prepared by varying the immersion time in the Au NP solution. An absorption spectrum of a Au NP layer with a concentration of $c_{Au} = 0.11 \times 10^{17}$ m^{-2} is shown in Figure 1.

Five different sizes of TGA stabilized CdTe QDs were used, and the diameters are given in Table 1. Reference monolayers of the QDs are prepared by depositing the QDs directly on a polyelectrolyte buffer layer on a quartz substrate. The monolayer PL emission peak (λ_{em}) varies from 534 to 660 nm with increasing QD size, as shown in Figure 1. The emission of the smaller, green emitting QDs is close to the resonance of the LSP absorption peak of the Au NP layer. As the size of the QDs increases the emission is red-shifted with respect to the LSP peak. To complete the QD–Au NP bilayer structures, the QD layers are deposited on a polyelectrolyte spacer layer covering the Au NP

TABLE 1. Properties of the QDs: Central Emission Wavelength (nm), Diameter (nm) and QY of the QD Monolayers on Quartz[a]

	QD-1	QD-2	QD-3	QD-4	QD-5
central emission wavelength (nm)	534	547	559	623	660
QD diameter (nm)	2.55	2.6	2.7	3.3	3.4
quantum yield, QY	3.5%	3.5%	6%	11%	6%
spectral overlap, J (10^{17} nm^4/(cm·M))	3.4	3.3	3.3	3.0	2.5
calculated R_0 (nm)	(6.9 ± 0.5)	(6.7 ± 0.5)	(7.5 ± 0.5)	(8.0 ± 0.5)	(7.0 ± 0.5)
experimental R_0 (nm)	(6.7 ± 0.6)	(6.2 ± 0.6)	(9.4 ± 0.8)	(9.9 ± 0.7)	(9.5 ± 0.8)
calculated d_0 (nm)	(3.3 ± 0.4)	(3.4 ± 0.4)	(3.8 ± 0.5)	(4.7 ± 0.5)	(4.2 ± 0.5)
experimental d_0 (nm)	(3.7 ± 0.6)	(3.5 ± 0.6)	(5.7 ± 0.8)	(5.7 ± 0.7)	(5.5 ± 0.8)

[a] The calculated R_0 is determined from eq 3 using the spectral overlap, J, and quantum yield, QY. The calculated d_0 is determined from eq 7 using the central emission wavelength and quantum yield, QY. The experimental R_0 and d_0 are the averages of the values obtained from fitting the distance and Au NP concentration dependences.

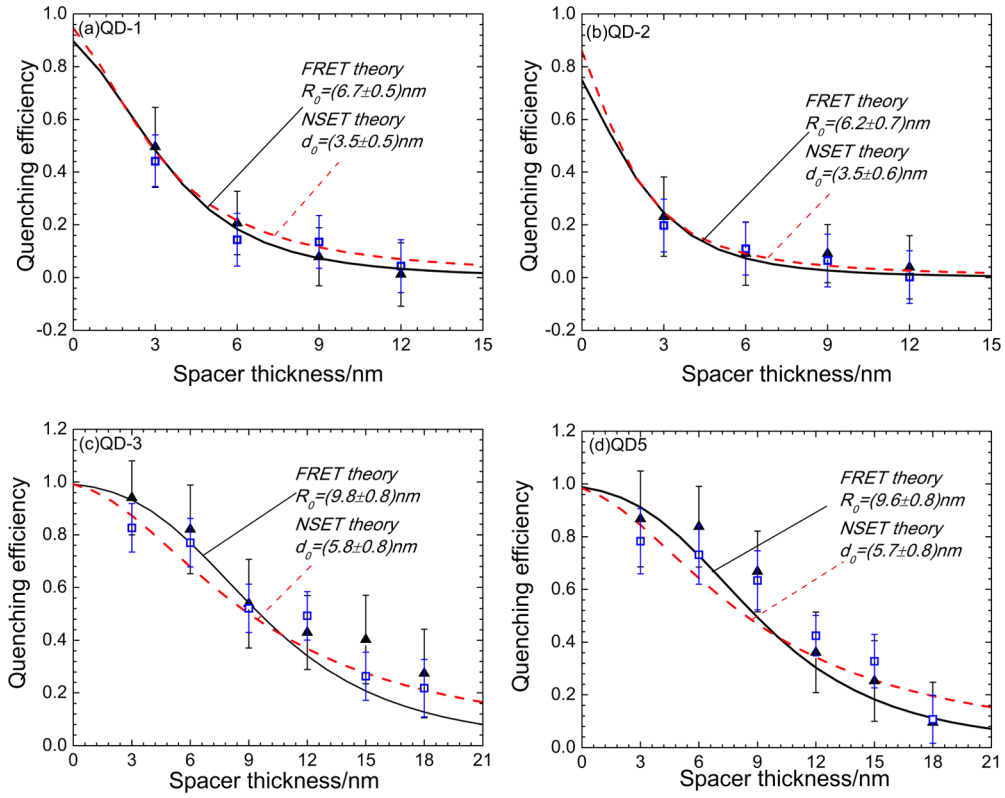

Figure 2. Distance dependence of the quenching efficiency, *E*, of QD monolayers deposited on top of a Au NP monolayer. The PL quenching efficiency was determined from the integrated PL spectra for the overall ensemble emission (solid black triangle) and the lifetime quenching was determined from the average decay lifetimes (open blue square). The solid line (black) represents the fit of the quenching efficiency with a model based on the FRET mechanism. The dashed line (red) represents the fit of the quenching efficiency with a model based on the NSET mechanism. (a) QD-1 λ_{em} = 534 nm, (c_{Au} = (0.16 ± 0.01) × 10^{17} m^{-2}); (b) QD-2 λ_{em} = 547 nm, (c_{Au} = (0.09 ± 0.01) × 10^{17} m^{-2}); (c) QD-3 λ_{em} = 559 nm, (c_{Au} = (0.21 ± 0.03) × 10^{17} m^{-2}); and (d) QD-5 λ_{em} = 660 nm, (c_{Au} = (0.26 ± 0.04) × 10^{17} m^{-2}).

layer. The QYs of the QDs in the layers are given in Table 1.

The quenching of the QD emission through interaction with the Au NP layer was characterized using the PL spectral quenching and the lifetime quenching. The PL quenching, $Q_{PL} = 1 - I_{onAu}/I_{QD}$, was calculated from the integrated spectral emission of the QD reference monolayer, I_{QD}, and that of the layers deposited on top of gold NP layers, I_{onAu}. The lifetime quenching, $Q_{LT} = 1 - \tau_{onAu}/\tau_{QD}$, was calculated from the PL decay times of the QD reference monolayer, τ_{QD}, and the QD layer on top of the Au NP layer, τ_{onAu}. The average lifetimes were determined from biexponential fits of the time-resolved PL traces.[27,28] The QD reference monolayer has the same QD concentration, to take account of the QD concentration dependence of the PL lifetime of monodispersed QD monolayers.[27]

The distance dependent quenching, as a function of the polyelectrolyte spacer layer thickness, is shown for four QDs in Figures 2a–d. The Au NP concentration was adjusted slightly to achieve a similar quenching range for the different QDs. The Au NP concentration dependence of the quenching efficiency is fully examined in the next section. The polyelectrolyte spacer layer thickness, verified using an X-ray diffraction technique,[28] was varied from 3 to 18 nm. For all QDs the PL emission quenching increases as the separation between the QD and Au NP monolayers is reduced, and the lifetime shortens more as the QD monolayer is brought in closer proximity to the Au NP layer. First, it can be noted that there is close agreement of the PL quenching with the lifetime quenching indicating that the change in the QD PL and lifetime is due only to changes in the nonradiative rate, through the introduction of the additional mechanism of energy transfer to the Au NPs, and that the QD radiative rate, k_r, is unchanged.[29] It is also expected that the intrinsic nonradiative rate, k_{nr}, of the QD is unaffected by the QD–Au NP interaction.[30] Therefore, the PL and lifetime quenching are signatures of the nonradiative energy transfer mechanism from the QD to the Au NP layer and the energy transfer efficiency is $E = Q_{PL} = Q_{LT}$.

The separation dependence can first be analyzed within the FRET model. The experimental FRET efficiency can be fitted using eq 5. As the center to center separation, *d*, and the Au NP concentration, c_{Au}, have been independently measured, the Förster radius, R_0, can be determined from the fit. The best fit is shown as a solid black line on each of the graphs in Figure 2, and the extracted Förster radii, R_0, are given on each graph.

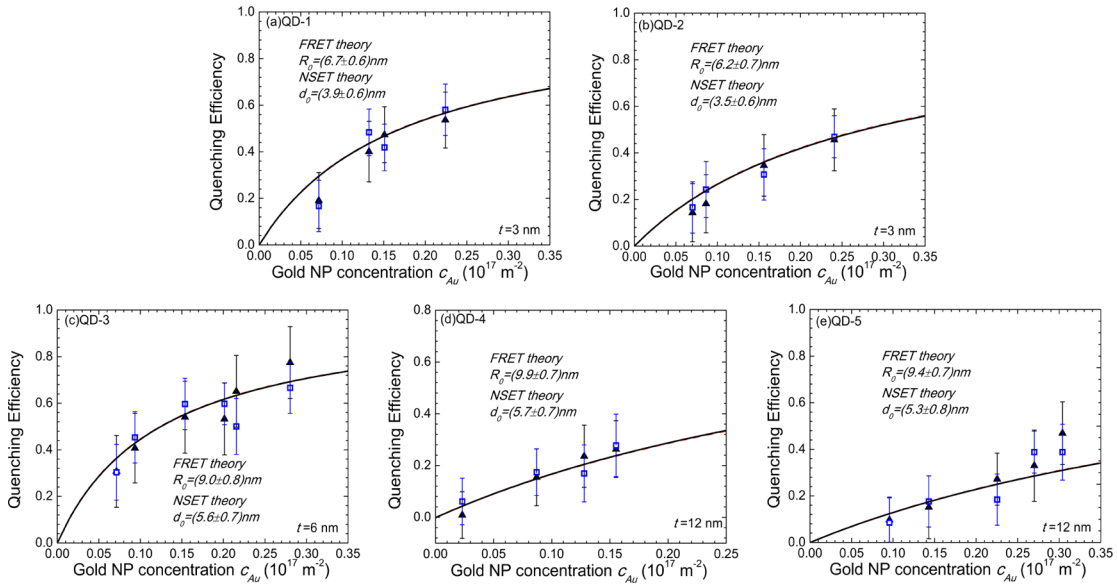

Figure 3. Au NP concentration dependence of the quenching efficiency, *E*, of QD monolayers deposited on top of a Au NP monolayer. The PL quenching efficiency was determined from the integrated PL spectra for the overall ensemble emission (solid black triangle) and the lifetime quenching was determined from the average decay lifetimes (open blue square). The solid line (black) represents the fit of the quenching efficiency with a model based on the FRET mechanism. The fit of the quenching efficiency with a model based on the NSET mechanism overlaps the fit from the FRET model. (a) QD-1 λ_{em} = 534 nm, (b) QD-2 λ_{em} = 547 nm, (c) QD-3 λ_{em} = 559 nm, (d) QD-4 λ_{em} = 623 nm, and (e) QD-5 λ_{em} = 660 nm.

First, it can be noted that the trend of the experimental data can be well predicted by the form of eq 5. Second, Förster radii greater than 6 nm are observed in all cases. These are relatively large values compared to the Förster radii determined for FRET between donor and acceptor QDs for solid-state structures at room temperature,[27,28,31] but similar to the characteristic interaction distances reported for energy transfer from QDs to 1.4 nm gold NPs.[5] It can also be noted that the measured Förster radius is larger for the off-resonance QDs red-shifted from the LSP resonance. This would suggest that the gold nanoparticle−QD interaction is stronger for QDs red-shifted with respect to the LSP resonance rather than in resonance.

The Au NP concentration dependence of the PL and lifetime quenching is shown in Figure 3a−e. The Au NP concentration was varied from approximately 0.05 × 10^{17} m^{-2} to 0.35 × 10^{17} m^{-2}. The polyelectrolyte spacer layer thickness, *t*, is indicated on each plot. As the strength of QD−Au NP interaction varies for the different QD species, the spacer layer thickness was adjusted to have similar quenching efficiencies for all five QDs over the concentration range. Again, there is close agreement of the PL and lifetime quenching data, as was observed for the distance dependent data. The Förster radius of each QD−Au NP pair can be extracted by fitting with eq 5. The center to center separation, *d*, is known for each pair. The best fit is shown as the solid black line on each of the plots in Figure 3, and the extracted Förster radii, R_0, are also given on each graph. First, similar to what was observed for the separation dependence of the energy transfer efficiency, the trend of the experimental data is in good agreement with the FRET model, and second, there is close agreement between the Förster radii determined from the concentration and separation dependences for QD-1, QD-2, QD-3, and QD-5. The average R_0 value for each QD is given in Table 1. To provide an additional data point for the wavelength dependence of the quenching, the Au concentration dependence for QD-4, with central emission wavelength at 623 nm, has also been shown in Figure 3, and the R_0 extracted from the fit is included in Table 1.

Furthermore, using eq 3, R_0 can be estimated from the spectral overlap of the area-normalized donor (QD) emission spectrum, $\hat{I}_D(\lambda)$, and the acceptor (LSP) extinction spectrum, $\varepsilon_{AuNP}(\lambda)$, which can be obtained by scaling the absorption spectrum of the Au NPs to show a value of 4.19 × 10^6 M^{-1} cm^{-1} as the peak value of the surface plasmon resonance. The spectral overlap and QY for the QD monolayers is also given in Table 1, and the volume weighted refractive index is $n = (1.5 \pm 0.3)$. The calculated R_0 values can be compared with those obtained from fitting the separation and Au NP concentration dependence. The calculated R_0 shows a relatively small variation of approximately 1 nm over the full wavelength range. It is seen that for the QD-1 and QD-2, emitting close to the localized surface plasmon resonance, there is reasonable agreement between the R_0 values obtained from the fitting and those calculated. However, for QD-3, QD-4, and QD-5, with emission red-shifted from the LSP resonance, the R_0 values obtained from fitting the separation and Au NP concentration dependences are significantly larger

than those calculated from the spectral overlap. Therefore, analysis of the QD emission quenching within the FRET formalism does not provide good agreement between experiment and theory over the full wavelength range. Additionally, as mentioned earlier, the larger R_0 values imply that LSP−QD interaction, and consequently energy transfer from QDs to the Au NPs, is more efficient when the QD emission is red-shifted off the LSP resonance, contrary to expectations. This stronger interaction is also reflected in the increased separation between the off-resonance QD monolayers and the Au NP monolayer in order to obtain a similar level of quenching as for the on resonance QD bilayer samples. While the trends of the experimental data could be well reproduced by FRET theory, the characteristic interaction distance obtained from fitting the experimental data with theory does not agree with the value calculated from the spectral overlap over the full wavelength range. Therefore, NSET theory was considered as an alternative model to explain the distance and concentration dependences of the quenching efficiency.

To investigate the NSET mechanism for energy transfer to a plane of Au NPs, the separation and Au NP concentration data can be fitted using eq 9 with d_0 as the fit parameter. All other parameters have been independently measured, and in this case the relevant separation is from the center of the QD to the Au NP surface, $d-r_{Au}$. The best fits are shown as dashed lines in Figure 2 and Figure 3. The corresponding d_0 values are given on each graph. The dependence of E_{NSET} on the spacer layer thickness is clearly different to that of E_{FRET}; however, a good fit to the experimental data, within the measurement error, can be observed for all four QD species shown in Figure 2. As can be clearly seen from eqs 5 and 9, E_{NSET} has the same Au NP concentration dependence as E_{FRET}, and, therefore, the fits overlay each other in Figure 3. There is good agreement between the d_0 values extracted from the separation and Au NP concentration dependences, and the average values for each QD are given in Table 1.

The d_0 values extracted from the fitting can be compared with those calculated using eq 7. The QD emission frequency is calculated using the central emission wavelength and QD monolayer quantum yield, given in Table 1. The calculated d_0 values for each of the five QDs are also given in Table 1. It can be seen that the fitting and calculated values are in closer agreement across the entire wavelength range than is found using FRET analysis. In particular, the values for QD-1 and QD-2, emitting close the localized surface plasmon peak, agree within the experimental error.

At this point it can be noted that we have not considered the Au monolayer itself as an infinite surface, in which case the energy transfer rate would be given by eq 6 and the surface energy transfer efficiency would be described by $E = 1/(1 + ((d - r_{Au})/d_0)^4)$. Such an approach would neglect the observed strong Au NP concentration dependence observed in the bilayer structures. Instead, this is the form of the NSET transfer efficiency for a single emitter−Au NP pair.[4] However, it is worth commenting that the d_0 values obtained by fitting the separation and concentration dependent data with this expression also show a large discrepancy with the calculated values for the three off-resonance QDs, similar to what was observed using the FRET analysis.

CONCLUSIONS

Five different-sized CdTe QDs have been used to probe the wavelength dependence of emission quenching of a QD monolayer deposited in proximity to a plane of 5.5 nm diameter Au NPs. Strong QD emission quenching is observed for QDs red-shifted by 120 nm from the peak of the LSP resonance. We have shown that while the distance and Au NP concentration dependences of the quenching efficiencies for all five QDs follow trends that can be fitted with a model for FRET between two planes, the extracted Förster radii do not agree with expected values for QDs emitting off the LSP resonance. Agreement within experimental error is only observed for QDs emitting close to the LSP peak. Analysis using a NSET model for the QD−Au NP interaction can also predict the trends of the separation and Au NP concentration dependences of the nonradiative energy transfer. It is found that closer agreement between the extracted characteristic distance, d_0, and the theoretically expected value is observed over the full wavelength range. While further theoretical studies are required to explain the approximation of MNPs of such small dimensions as infinite surfaces within the NSET approach, this experimental study suggests that the NSET formalism can be a convenient phenomenological tool for the analysis of emission quenching due to nonradiative energy transfer to a plane of metal NPs.

METHODS

Bilayer structures with QDs and Au NPs were prepared by a layer-by-layer deposition technique. Details on the polyelectrolytes and concentrations used can be found elsewhere.[27] Colloidal Au NPs with an average diameter of 5.5 nm stabilized by 4-dimethylaminopyridine (DMAP)[32] were deposited first on a polyelectrolyte buffer layer covering a quartz slide. To achieve different Au NP concentrations in the layer the immersion time in the Au NP solution, with a concentration of the order of 1×10^{-7} M, was varied between 1 and 20 min. The fitting of the solution spectra[33,34] gave a molar extinction coefficient of 4.19×10^6 M^{-1} cm^{-1} at the wavelength of the LSP absorption peak, which was used to estimate the gold NP concentration from the Au NP layer absorption spectra.

The CdTe QDs, stabilized by thioglycolic acid, were synthesized in water according to standard procedures.[35,36] To make the QD−Au NP bilayer structures, the QD layers are deposited on a polyelectrolyte spacer layer covering the Au NP layer.

The QYs of the QDs in the layers were determined in comparison to the luminescent standard Rhodamine 6G. The measured QYs in the monolayers have been validated by comparison of the theoretical and experimentally measured separation and concentration dependencies of FRET between donor and acceptor nanocrystal QDs. The theoretical dependencies were calculated using the measured QYs of the QDs in monolayers.[28,37]

A Shimadzu UV-2401 PC double-beam UV−vis recording spectrometer was used to measure the absorption spectra of the layer structures. The room temperature PL spectra of the samples were recorded with a Perkin-Elmer LS 55 fluorescence spectrometer using an excitation wavelength of 400 nm. The time-resolved PL decays were measured with a PicoQuant Microtime200 time-resolved confocal microscope system for an excitation wavelength of 470 nm and an average excitation power of 16 nW. The emission signal of the QD monolayers was recorded by scanning an area of 80 μm × 80 μm (150 × 150 pixels) with a repetition rate of 10 MHz and an integration time of 4 ms per pixel.

Conflict of Interest: The authors declare no competing financial interest.

Acknowledgment. This work was financially supported by Science Foundation Ireland project 10/IN.1/12975. N. Gaponik and A. Rogach acknowledge support by a grant from the Germany/Hong Kong Joint Research Scheme sponsored by the Research Grants Council of Hong Kong and the German Academic Exchange Service (Reference No.: G_HK008/10).

REFERENCES AND NOTES

1. Li, X; Qian, J.; Jiang, L.; He, S. Fluorescence Quenching of Quantum Dots by Gold Nanorods and Its Application to DNA Detection. *Appl. Phys. Lett.* **2009**, *94*, 063111.
2. Mayilo, S.; Kloster, M. A.; Wunderlich, M.; Lutich, A.; Klar, T. A.; Nichtl, A.; Kürzinger, K.; Stefani, F. D.; Feldmann, J. Long-Range Fluorescence Quenching by Gold Nanoparticles in a Sandwich Immunoassay for Cardiac Tropponin T. *Nano Lett.* **2009**, *9*, 4558–4563.
3. Lee, J.; Hernandez, P.; Lee, J.; Govorov, A. O.; Kotov, N. A. Exciton-Plasmon Interactions in Molecular Spring Assemblies of Nanowires and Wavelength-Based Protein Detection. *Nat. Mater.* **2007**, *6*, 291–295.
4. Jennings, T. L.; Singh, M. P.; Strouse, G. F. Flourescent Lifetime Quenching Near *d*=1.5 nm Gold Nanoparticles. *J. Am. Chem. Soc.* **2006**, *128*, 5462–5467.
5. Pons, T.; Medintz, I. L.; Sapsford, K. E.; Higashiya, S.; Grimes, A. F.; English, D. S.; Mattoussi, H. On the Quenching of Semiconductor Quantum Dot Photoluminescence by Proximal Gold Nanoparticles. *Nano Lett.* **2007**, *7*, 3157–3164.
6. Yun, C. S.; Javier, A.; Jennings, T.; Fisher, M.; Hira, S.; Peterson, S.; Hopkins, B.; Reich, N. O.; Strouse, G. F. Nanometal Surface Energy Transfer in Optical Rulers, Breaking the FRET Barrier. *J. Am. Chem. Soc.* **2005**, *127*, 3115–3119.
7. Förster, T. Zwischenmolekulare Energiewanderung und Fluoreszenz. *Ann. Phys.* **1948**, *2*, 55–75.
8. Stryer, L.; Haugland, R. P. Energy Transfer—A Spectroscopic Ruler. *Proc. Natl. Acad. Sci.* **1967**, *58*, 719–726.
9. Chhabra, R.; Sharma, J.; Wang, H.; Zou, S.; Lin, S.; Yan, H.; Lindsay, S.; Liu, Y. Distance-Dependent Interactions between Gold Nanoparticles and Fluorescent Molecules with DNA as Tunable Spacers. *Nanotechnology* **2009**, *20*, 485201.
10. Acuna, G. P.; Bucher, M.; Stein, I. H.; Steinhauer, C.; Kuzyk, A.; Holzmeister, P.; Schreiber, R.; Moroz, A.; Stefani, F. D.; Liedl, T.; *et al.* Distance Dependence of Single Fluorophore Quenching by Gold Nanoparticles Studied on DNA Origami. *ACS Nano* **2012**, *6*, 3189–3195.
11. Singh, M. P.; Strouse, G. F. Involvement of the LSPR Spectral Overlap for Energy Transfer between a Dye and Au Nanoparticle. *J. Am. Chem. Soc.* **2010**, *132*, 9383–9391.
12. Chowdhury, S.; Zhikun, W.; Jaquins-Gerstl, A.; Liu, S.; Dembska, A.; Armitage, B. A.; Rongchao, J.; Peteanu, L. A. Wavelength Dependence of the Fluorescence Quenching Efficiency of Nearby Dyes by Gold Nanoclusters and Nanoparticles: The Roles of Spectral Overlap and Particle Size. *J. Phys. Chem. C* **2011**, *115*, 20105–20112.
13. Haldar, K. K.; Sen, T.; Patra, A. Metal Conjugated Semiconductor Hybrid Nanoparticle-Based Fluorescence Resonance Energy Transfer. *J. Phys. Chem. C* **2010**, *114*, 4869–4874.
14. Batabyal, S.; Makhal, A.; Das, K; Raychaudhuri, A. K.; Pal, S. K. Ultrafast Dynamics of Excitons in Semiconductor Quantum Dots on a Plasmonically Active Nano-Structured Silver Film. *Nanotechnology* **2011**, *22*, 195704–195704.
15. Viste, P.; Plain, J.; Jaffoil, R.; Vial, A.; Adam, P. M.; Royer, P. Enhancement and Quenching Regimes in Metal-Semiconductor Hybrid Optical Nanosources. *ACS Nano* **2010**, *4*, 759–764.
16. Clapp, A. R.; Medintz, I. L.; Mattoussi, H. Förster Resonance Energy Transfer Investigations Using Quantum-Dot Fluorophores. *ChemPhysChem* **2006**, *7*, 47–57.
17. Resch-Genger, U.; Grabolle, M.; Cavaliere-Jaricot, S.; Nitschke, R.; Nann, T. Quantum Dots *versus* Organic Dyes as Fluorescent Labels. *Nature Methods* **2008**, *5*, 763–775.
18. Wargnier, R.; Baranov, A. V.; Maslov, V. G.; Stsiapura, V.; Artemyev, M.; Pluot, M.; Sukhanova, A.; Nabiev, I. Energy Transfer in Aqueous Solutions of Oppositely Charged CdSe/ZnS Core/Shell Quantum Dots and in Quantum Dot−Nanogold Assemblies. *Nano Lett.* **2004**, *4*, 451–457.
19. Chandramohan, S.; Ryu, B. D.; Uthirakumar, P.; Wang, H. J.; Kim, H. K.; Kim, H. G.; Hong, C.-H. Tuning the Spectrometric Properties of White Light by Surface Plasmon Effect Using Ag Nanoparticles in a Colour Converting Light-Emitting Diode. *Solid-State Electron.* **2011**, *57*, 90–92.
20. Lesnyak, V.; Wolf, A.; Dubavik, A.; Borchardt, L.; Voitekhovich, S. V.; Gaponik, N.; Kaskel, S.; Eychmüller, A. 3D Assembly of Semiconductor and Metal Nanocrystals: Hybrid CdTe/Au Structures with Controlled Content. *J. Am. Chem. Soc.* **2011**, *133*, 13413–13420.
21. Lunz, M.; Gerard, V. A.; Byrne, S. J.; Gun'ko, Y. P.; Lesnyak, V.; Gaponik, N.; Susha, A. S.; Rogach, A. L.; Bradley, A. L. Surface Plasmon Enhanced Energy Transfer between Donor and Acceptor CdTe Nanocrystals Quantum Dot Monolayers. *Nano Lett.* **2011**, *11*, 3341–3345.
22. Ozel, T.; Nizamoglu, S.; Sefunc, M. A.; Samarskaya, O.; Ozel, I. O.; Mutugun, E.; Lesnyak, V.; Gaponik, N.; Eychmüller, A.; Gaponenko, S. V.; *et al.* Anisotropic Emission from Multi-Layered Plasmon Resonator Nanocomposites of Isotropic Semicondcutor Quantum Dots. *ACS Nano* **2011**, *5*, 1328–1334.
23. Lakowicz, J. R. *Principles of Fluorescence Spectroscopy*; Kluwer Academic/Plenum: New York, 1999.
24. B. W. Van der Meer, Coker, G.; , Chen, S. Y. S. *Resonance Energy Transfer: Theory and Data*; VCH: New York, 1994.
25. Rogach, A. L.; Klar, T. A.; Lupton, J. M.; Meijerink, A.; Feldmann, J. Energy Transfer with Semiconductor Nanocrystals. *J. Mater. Chem.* **2009**, *19*, 1208–1221.
26. Persson, B. N. J.; Lang, N. D. Electron-Hole Pair Quenching of Excited States Near a Metal. *Phys. Rev. B* **1982**, *26*, 5409–5415.
27. Lunz, M.; Bradley, A. L.; Chen, W.-Y.; Gerard, V. A.; Byrne, S. J.; Gun'ko, Y. P.; Lesnyak, V.; Gaponik, N. Influence of Quantum Dot Concentration on Förster Resonant Energy Transfer in Monodispersed Nanocrystal Quantum Dot Monolayers. *Phys. Rev. B* **2010**, *81*, 205316.
28. Lunz, M.; Bradley, A. L.; Gerard, V. A.; Byrne, S. J.; Gun'ko, Y. P.; Lesnyak, V.; Gaponik, N. Concentration Dependence of Förster Resonant Energy Transfer between Donor and Acceptor Nanocrystal Quantum Dot Layers: Effect of Donor−Donor Interactions. *Phys. Rev. B* **2011**, *83*, 115423.
29. Schneider, G.; Decher, G. Distance-Dependent Fluorescence Quenching on Gold Nanoparticles Ensheathed with

Layer-by-Layer Assembled Polyelectrolytes. *Nano Lett* **2006**, *6*, 530–536.
30. Govorov, A. O.; Bryant, G. W.; Zhang, W.; Skeini, T.; Lee, J.; Kotov, N. A.; Slocik, J. M.; Naik, R. R. Exciton-Plasmon Interaction and Hybrid Excitons in Semiconductor–Metal Nanoparticle Assemblies. *Nano Lett.* **2006**, *6*, 984–9942006.
31. Kagan, C. R.; Murray, C. B.; Bawendi, M. G. Long-Range Resonance Transfer of Electronic Excitations in Close-Packed CdSe Quantum-Dot Solids. *Phys. Rev. B* **1996**, *54*, 8633–8643.
32. Gittins, D. I.; Caruso, F. Spontaneous Phase Transfer of Nanoparticulate Metals from Organic to Aqueous Media. *Angew. Chem.—Int. Ed.* **2001**, *40*, 3001–3004.
33. Jain, P. K.; Lee, K. S.; El-Sayed, I. H.; El-Sayed, M. A. Calculated Absorption and Scattering Properties of Gold Nanoparticles of Different Size, Shape and Composition: Applications in Biological Imaging and Biomedicine. *J. Phys. Chem. B* **2006**, *110*, 7238–7248.
34. Amendola, V.; Meneghetti, M. Size Evaluation of Gold Nanoparticles by UV–vis Spectroscopy. *J. Phys. Chem. C* **2009**, *113*, 4277–4285.
35. Byrne, S. J.; Corr, S. A.; Rakovich, T. Y.; Gun'ko, Y. K.; Rakovich, Y. P.; Donegan, J. F; Mitchell, S.; Volkov, Y. Optimisation of the Synthesis and Modification of CdTe Quantum Dots for Enhanced Live Cell Imaging. *J. Mater. Chem.* **2006**, *16*, 2896–2902.
36. Rogach, A. L.; Franzl, T.; Klar, T. A.; Feldmann, J.; Gaponik, N.; Lesnyak, V.; Shavel, A.; Eychmüller, A.; Rakovich, Y. P.; Donegan, J. F. Aqueous Synthesis of Thiol-Capped CdTe Nanocrystals: State-of-the-Art. *J. Phys. Chem. C* **2007**, *111*, 14628–14637.
37. Lunz, M.; Bradley, A. L.; Chen, W.-Y.; Gun'ko, Y. P. Two-Dimensional Förster Resonant Energy Transfer in a Mixed Qauntum Dot Monolayer: Experiment and Theory. *J. Phys. Chem. C* **2009**, *115*, 3084–3088.